Natural Hazards (2023) 118:1117–1136
https://doi.org/10.1007/s11069-023-06040-8

ORIGINAL PAPER

Submarine landslide tsunami hazard assessment for the western Makran based on a deterministic approach

Mohammadsadegh Nouri[1,2] · **Amin Rashidi**[3] · **Masoud Montazeri Namin**[1] · **Dan H. Shugar**[4]

Received: 27 August 2021 / Accepted: 25 May 2023 / Published online: 10 June 2023

Abstract

The Makran region, which borders southern Iran and Pakistan along the Gulf of Oman, has experienced multiple tsunamis in the last century, with some being triggered by submarine landslides. However, the role played by submarine landslides has been largely neglected in tsunami hazard assessments in the western Makran. In the present study, four different submarine landslide scenarios with volumes of 10–40 km^3 are simulated on 25 locations in the western Makran, resulting in 100 different hypothetical scenarios. The results indicate that Oman's coastline, a country in the western part of Makran subduction zone, is more vulnerable to the hazard of landslide-generated waves (maximum average of 3.1 m wave height) compared to Iran (maximum average 0.9 m height). Although Chabahar, Iran, and Muscat, Oman, two major cities in the region, experienced severe waves during some scenarios, it can be implied Muscat is more vulnerable to this kind of tsunami due to the significant gap between the maximum and average wave height for all scenarios. We further discuss that applying hypothetical worst-case scenarios can sometimes lead to an overestimation in tsunami hazard assessment. Therefore, more geological, sedimentological, and geotechnical considerations and studies are required for defining submarine landslide worst-case scenarios.

Keywords Submarine landslide · Tsunami · Hazard assessment · Numerical modeling · Western Makran

✉ Mohammadsadegh Nouri
msnouri@udel.edu

[1] Department of Civil Engineering, University of Tehran, Tehran, Iran

[2] Present Address: Center for Applied Coastal Research, University of Delaware, Newark, DE 19716, USA

[3] Univ. Grenoble Alpes, Univ. Savoie Mont Blanc, CNRS, LAMA, 73000 Chambéry, France

[4] Water, Sediment, Hazards, and Earth-Surface Dynamics (waterSHED) Lab, Department of Geoscience, University of Calgary, Calgary, Canada

1 Introduction

Tsunamis are most often triggered by earthquakes, volcanic eruptions and submarine landslides (Higman et al. 2018; Heidarzadeh et al. 2022;). During the past decades, the effect of submarine landslides was generally neglected by researchers while developing tsunami hazard mitigation plans. After the 1998 Papua New Guinea landslide tsunami, which caused at least 2200 fatalities (Synolakis et al. 2002), several national agencies started evaluating the potential of submarine landslides as a serious threat and have made substantial progress toward tsunami preparedness against landslide-generated waves (Heidarzadeh and Satake 2015, 2017b; Pranantyo et al. 2021).

For a better understanding of coastal impacts to tsunamis, there are three common approaches for conducting a tsunami hazard assessment:

1. Deterministic approach: In this method, actual or hypothetical landslides are defined as the worst-case events (in terms of largest generated waves), and the wave heights and run-ups are calculated in the vicinity of coastal cities. By employing this method, we can produce inundation maps for coastal regions, including vulnerable communities. Although employing this method may necessitate days of computation on high-performance computing facilities, it is still one of the most favored approaches among tsunami modelers thanks to its straightforward steps. However, it is challenging to presume some hypothetical, yet valid worst-case scenarios in this approach. This method was employed to conduct landslide tsunami hazard assessment in different parts of the world (Geist et al. 2009; Gylfadóttir et al. 2017; Lindhorst et al. 2014; Schwab et al. 2014; Tan et al. 2018; Urgeles et al. 2019; Rauter et al. 2022;).
2. Probabilistic approach: This method, which is inspired by the probabilistic seismic hazard assessment (Grezio et al. 2017), can determine the likelihood of a tsunami with certain wave height and recurrence intervals within a given time period at a particular location. This is simply done by numerical models of tsunamis combined with source probabilities to quantitatively estimate the probability of exceedance of different levels of wave amplitude by expressing it in a hazard curve. Since landslide data usually do not provide equally good statistics as earthquake data, applying such an approach involves various challenges, including the uncertainty in the landslide mean return period. Moreover, having a comprehensive and broad range of data about previous events is critical to the successful application of probabilistic models. However, this method has been successfully undertaken to prioritize high hazard locations (Grilli et al. 2009; Pampell-Manis et al. 2016; Salmanidou et al. 2019; Løvholt et al. 2020; Iorio et al. 2021).
3. Machine-learning approach: This nascent method employs machine-learning algorithms to estimate tsunami inundation in real time. Compared with the former approaches, this method is markedly faster and can produce rapid tsunami inundation forecasts with satisfying accuracy. Mulia et al. (2018) successfully implemented this approach to produce the inundation map during the 2011 Tohoku tsunami. Fauzi and Mizutani (2020) employed a couple of machine-learning algorithms to estimate tsunami inundation in the Nankai region. Mulia et al. (2020) used a deep-learning algorithm and forecasted inundation heights in some locations during the 2011 Tohoku tsunami. All of the mentioned articles above have considered earthquakes as the main cause of tsunami and tried to forecast the inundation. However, it is expected that these data-driven models will become a standard and popular model for tsunami hazard assessments with diverse types of sources in the near future.

Among the described approaches, applying a probabilistic approach requires an extensive range of data of previous events. Due to unavailability of high-resolution bathymetry data in Makran domain, it is not appropriate to employ this method for landslide-induced tsunamis (Harbitz et al. 2014). On the other hand, the machine-learning approach, although being fast and accurate for earthquake-triggered tsunamis, has not been well-validated regarding the landslide tsunami hazard assessment. Hence, the deterministic method can be the best way to evaluate the hazard of landslide-generated waves in this zone.

Makran has been a focus of several tsunami hazard assessments (e.g., Hoechner et al. 2016; Rashidi et al., 2022; Zafarani et al. 2023). Most of those studies have been performed for earthquake-generated tsunamis. However, tsunami researchers have recently paid more attention to the significance of landslide tsunamis in this region. Rodriguez et al. (Rodriguez et al. 2013) simulated a submarine landslide of 40 km^3 located within the Owen Ridge in the Arabian Sea and observed that it can produce wave heights up to 2.5 m on Oman's coastline. Rastgoftar and Soltanpour (2016) simulated a voluminous submarine landslide tsunami as the possible secondary tsunami source for the November 1945 tsunami in Makran. Heidarzadeh and Satake (2014) conducted several analyses over different source types for the September 2013 tsunami in Makran using spectral analysis and backward tsunami ray tracing. They concluded that a submarine slump should have contributed to the observed tsunami waves. Heidarzadeh and Satake (2017a) showed that adding a landslide source (with a length and width of 15 km and a thickness of 600 m) to the already proposed tectonic source (Heidarzadeh and Satake 2015) could generate the observed waves of the 1945 Makran tsunami. Supparsi et al. (2016) and Latcharote et al. (2018) investigated the effect of subaerial landslides in the Persian Gulf. Salmanidou et al. (2019) conducted a landslide tsunami hazard assessment in eastern Makran by simulating 60 slump scenarios and used their results to train a statistical emulator to predict 500,000 hypothetical scenarios for a probabilistic hazards assessment.

In this paper, we employ a scenario-based approach to conduct a landslide tsunami hazard assessment in the western part of Makran. Due to the scarcity of detailed historical records of previous submarine evidences in western Makran, we assume some hypothetical, feasible scenarios to evaluate the maximum wave heights. Afterward, we simulate the propagation of landslide-generated waves to better understand the coastal hazard in the zone.

2 Historical background

Makran region has been affected by a number of tsunamis in the past, originating from different sources. Most of the tsunamis that occurred in the region over the last millennium were triggered by earthquakes (Rashidi et al. 2020). Heidarzadeh et al. (2008) compiled a comprehensive list of tsunamis that occurred in MSZ. Although there is little historical records of submarine landslides or other mass movements in the MSZ, recent studies have suggested that some tsunamis in this region were accompanied by submarine mass movements (Hoffmann et al. 2014; Haider et al. 2023). There are only two instrumentally recorded tsunamis that are attributed to submarine landslides. First, the Makran tsunami on November 27, 1945, triggered by an M_w 8.0–8.3 earthquake, caused extensive damage and a death toll of 300 in the near field (Okal et al. 2015). Pendse (Pendse, 1946) reported that the near-field run-up observed on the Pasni coastline of southern Pakistan was between 12 and 15 m, which is very large for such an earthquake. Heidarzadeh and Sakate (2015,

2017a) concluded via numerical modeling that only a submarine landslide would be capable of producing the observed run-up.

The second earthquake was an inland earthquake in the province of Baluchistan, southwestern Pakistan, on September 24, 2013 (Hoffmann et al. 2014). Although the *Mw* 7.7 earthquake was large enough to produce considerable inundation, Heidarzadeh and Satake (2014) showed that none of the co-seismic crustal deformations could be the source for run-up observed at the Oman Sea. They concluded that a submarine slump with a source dimension of about 10–15 km and a thickness of about 100 m could be the source of the tsunami. Source locations for these two submarine landslides and their associated earthquakes are illustrated in Fig. 1.

Due to differences in seismicity and tectonics of the western and eastern halves of the MSZ, segmentation has been suggested for this zone. Historical records indicate that almost all major events have occurred in the eastern Makran. Most of the geological studies have focused on the eastern part of Makran since it has been seismically more active compared to the western part. It is not clear whether the western zone is naturally aseismic or silently accumulating energy over time to produce potential tsunamigenic earthquakes in near future. Frohling and Szeliga (2016) combined the GPS measurements of 20 stations in the region and concluded that western Makran sounds to be locked at a depth of at least 38 km and it is accumulating strain. They concluded that MSZ is capable of producing earthquakes up to M_w 8.8. Makran has one of the largest accretionary wedges on the earth and is distinguished by a 7-km-thick sedimentary layer (Kopp et al., 2000). According to reports by Byrne et al. (Byrne et al., 1992), the forearc's seaward 70 km are comprised of recently accreted, unconsolidated, and semi-consolidated sediments with low seismic velocities and high pore fluid pressures. These sediments have the potential to fail and cause massive tsunamigenic submarine landslides. In fact, seismic activity of

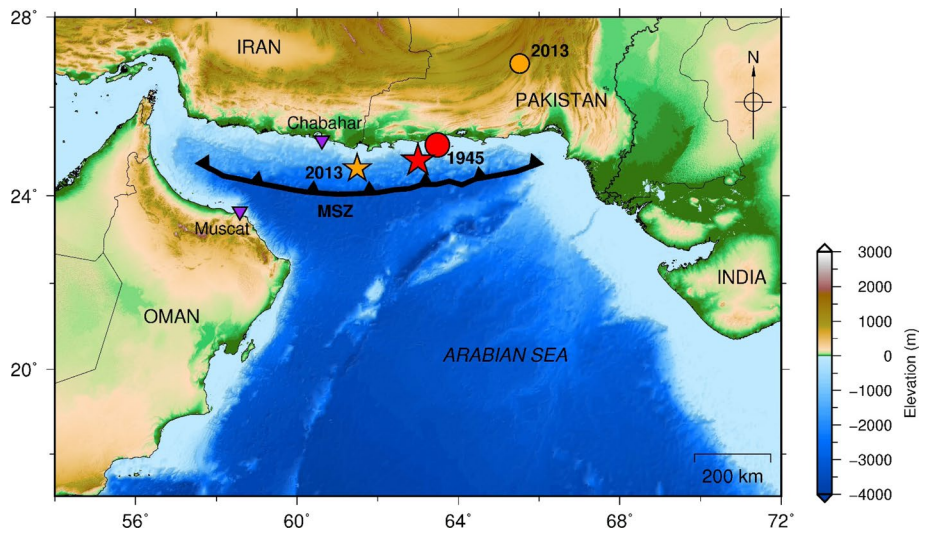

Fig. 1 Map of Makran subduction zone (MSZ). The red and orange circles represent the epicenter of the Makran earthquake of 27 November 1945 and the Pakistan earthquake of 24 September 2013. The red and orange stars locate the potential source locations of submarine landslides during the 1945 and the 2013 events, respectively (Heidarzadeh and Satake 2014, 2015, 2017a). The purple triangles are the locations of artificial tide gauges during the simulation

MSZ, along with a large accretionary wedge of sediments, large sedimentation and also erosion rates, are some of the factors that can provide the condition for any kind of submarine landslides in near future in this region (Kukowski et al. 2001; Heidarzadeh et al. 2008; ten Brink and Geist 2021). In addition, numerous external factors like climate changes or glacial cycles should be investigated to understand whether or not a region is susceptible to submarine landslides. The 1945 and 2013 tsunamis, which may have been generated by submarine landslides, can be considered preliminary evidence that the region is prone to submarine mass failures even following low seismic activity. This concept has also been previously reported by some authors based on geological and sedimentological investigations in the region (Bourget et al. 2010; Grando and Mcclay 2007). Even assuming that the western Makran is incapable of producing large offshore megathrust earthquakes, the 2013 earthquake could be an example denoting inland shakings can cause landslide-generated tsunamis in Makran.

There are some geological studies in MSZ that have shed some light on previous landslides in the region. Plat et al. (Platt et al. 1985) discussed that the active uplift and actual tensions on the Makran accretionary prism are the main cause of slumps and these slumps would become like turbidity currents in deeper sections. Kukowski et al. (2001) located several slumps in the eastern part of Makran. Ellouz et al. (2007) did a survey to acquire 3D bathymetry of the Makran accretionary prism offshore Pakistan and located various circular and linear slump scars. Grando and Mcclay (2007) discussed the structure of the Makran accretionary prism in offshore Southeastern Iran and inferred the occurrence of previous slumps using seismic interpretation. Mouchot et al. (2010) performed a geological survey in offshore Pakistan and explained that the slope instabilities appear to be frequent in the setting, however, with limited size. Bourget et al. (2010) also draw the same conclusion that the thick turbidity deposits in the region are because of the large slump or slide-triggered turbidity currents.

3 Methodology

3.1 Source modeling

To conduct a deterministic landslide-tsunami hazard assessment, researchers presume the past submarine landslides as the worst-case scenarios and simulate those events (Brune et al. 2010; Yalciner et al. 2014; Grilli et al. 2015). In order to apply a deterministic tsunami hazard assessment in western Makran, which has no conclusive evidence of past submarine mass movements, we must address two main obstacles: (a) determine locations that are prone to mass wasting and (b) estimate how extreme these events can be. To address the first challenge, we must keep in mind that there have been a wide variety of landslides all over the world that do not follow any specific pattern regarding their location, therefore makes it difficult to predict the susceptible locations. (Yavari-Ramshe and Ataie-Ashtiani 2016). The geological structure of eastern Makran is complicated for defining the mass failures as there are translational and rotational landslides because of the imbricate thrusts. It is not confirmed that the western Makran has the similar tectonic features such as imbricate thrusts. Additionally, the mass failures in western Makran can have different behaviors as the submarine landslides off Oman, a passive margin, can behave totally different from those off Iran and appear translational. To overcome these discrepancies for defining the landslide scenarios, we do not confine this hazard assessment to a single scenario and try

to presume different submarine landslide scenarios at different locations in the western part of Makran. Therefore, in this paper, we systematically locate hypothetical submarine landslides on a 0.5° structured grid, the same as hypothetical scenarios defined by Brune et al. (2010) (Fig. 2). We ignore locations with water depths less than 500 m since submarine landslides generally occur in intermediate depths (1000–2000 m) (Masson et al. 2006b; Harbitz et al. 2014). Although it is less likely that some of the scenarios in the deep ocean occur, there have been previous submarine mass failures like Tohoku 2011 (Tappin et al. 2014) that occurred in deep water and had generated significant tsunami waves. Therefore, we include locations in the deep ocean like 20, 21, and 23 to include the effect of landslide generated tsunami from sources in the deep ocean. Consequently, we model different landslides on 25 locations in western Makran, each of which involved different volume scenarios. Landslide directions are all downslope (Fig. 2). The slope angles are estimated using the GEBCO-2019 by converting the bathymetry data into grid format and dividing the change in elevation over the horizontal distance between the adjacent cells in the grid.

To address the second challenge, we must keep in mind that there are various types of submarine mass movements in nature, including translational and rotational failures (Locat and Lee 2002). In this work, we model rotational slumps because translational slides generally produce smaller wave amplitudes per unit volume, and results will be underestimated for a hazard assessment (Masson et al. 2006b). Additionally, the Makran seems to be more susceptible to submarine rotational slumps (Bourget et al. 2010; Grando and Mcclay 2007; Kukowski et al. 2001). Therefore, we assume four coherent rotational slumps for our scenarios, each of which contains different volumes, 10 to 40 km^3, all of which are in the range of previous possible candidate of landslides in the region (Heidarzadeh and Satake, 2014; Rastgoftar and Soltanpour 2016). At each of 25 source locations, we model four scenarios of different volumes. Details of the 25 source locations, including water depth at the

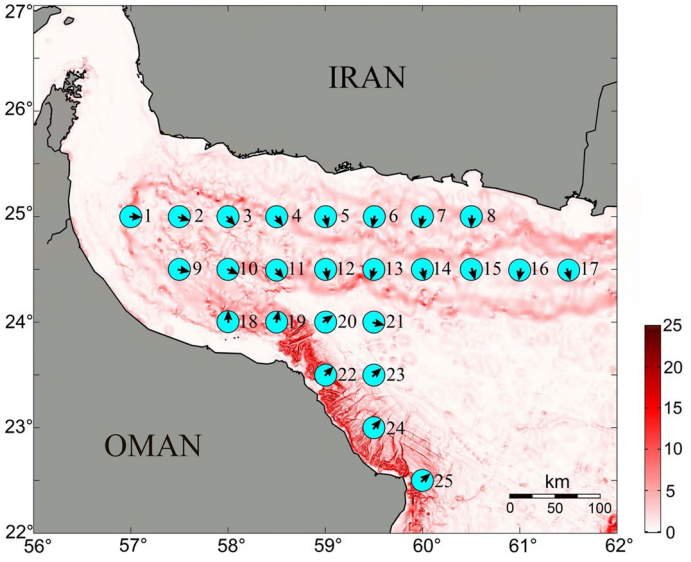

Fig. 2 Slope gradient map of Western Makran using the 15arcsec GEBCO-2019 bathymetry generated by Mirone (Luis 2007; Weatherall et al. 2015). The source location of our 25 scenarios are shown by cyan circles with their associated scenario number. The arrows inside the circles indicate the direction of mass movement during each scenario

Table 1 Ocean depth, slope angle, and azimuth angle of source locations (starting from East direction)

No.	Depth (m)	Slope angle (°)	Azimuth angle (°)	No.	Depth (m)	Slope angle (°)	Azimuth angle (°)
1	985	1.5	0	14	2492	1	288
2	1095	1	340	15	2294	3	292
3	1346	2.5	315	16	1950	3	260
4	1072	2	307	17	1810	1	284
5	860	1.5	280	18	907	4	90
6	918	2	268	19	1680	10	78
7	885	1.5	262	20	3310	0.7	52
8	792	6	270	21	3519	0.6	352
9	1475	1.5	348	22	1537	7	51
10	2390	4	334	23	3276	2	46
11	2070	8	315	24	1892	4	52
12	2476	4	281	25	1397	11	47
13	1850	5	244				

Table 2 Geometrical parameters for landslide scenarios in western Makran

No.	Length (km)	Width (km)	Thickness (km)	Approximate volume (km^3)
1	5	5	0.5	10
2	6.4	6.4	0.64	20
3	7.2	7.2	0.72	30
4	8	8	0.8	40

center of the slide, slope angle, and azimuth angle of slides, are shown in Table 1. A bulk density of 2150 kg m^{-3} was assumed for all of the slides to accurately simulate the submarine mass movements (Watts et al. 2003a, b; Heidarzadeh et al. 2019).

Table 2 provides the data for the landslide geometrical parameters of four different events, including slide length (B), width (w), maximum thickness (T). For each of the scenarios, we consider each landslide to have a Gaussian shape with radial symmetry and a constant width so that length and width are equal and ten times the thickness. By assuming a semielliptical shape for submarine mass movements, the volume is calculated by the formula $V = \pi wBT/4$ (Watts et al. 2005).

3.2 Numerical modeling

Numerical simulation of tsunamis comprises various stages. At first, the generation of tsunamis takes place by a submarine mass movement, which is a complex process that involves different hydro-sedimentary processes like fluid-particle and particle–particle interactions, complicating the numerical simulations. However, there are various approaches that solve real-world problems accurately and computationally efficiently (Heidarzadeh et al., 2014; Yalciner et al. 2014; Grilli et al. 2015;). Here, we take advantage of the previously proposed semi-empirical formulas (Grilli and Watts 2005; Watts et al. 2005) to create a 3D waveform:

$$\eta_{0,3D} = \left(\frac{w}{w+\lambda_0}\right)(0.0286T)(1-0.75\sin\theta)\left(\frac{bsin\theta}{d}\right)^{1.25} \quad (1)$$

$$\eta(x,y) = -\frac{\eta_{0,3D}}{\eta_{min}}\mathrm{sech}^2\left(\kappa\frac{y-y_0}{w+\lambda_0}\right)\left(\exp\left\{-\left(\frac{x-x_0}{\lambda_0}\right)^2\right\} - \kappa'\exp\left\{-\left(\frac{x-\Delta x-x_0}{\lambda_0}\right)^2\right\}\right) \quad (2)$$

In these equations, $\eta_{0,3D}$ is the characteristic 3D tsunami amplitude and is estimated from Eq. 1. The geometrical parameters of the slides are T, b, and w, representing the thickness, length, and width of the slide, respectively. The positioning parameters of the slides, x_0, y_0, d, and θ, are initial longitude, latitude, landslide submergence depth, and bed slope angle, respectively. The κ' and Δx parameters are used to control the double Gaussian shape of the initial condition. In this work, $\kappa' = 0.83$ and Δx, which is the distance between the crest and through of the surface elevation, is assumed to be 2. κ is also assumed to 3.

Since initial waveforms are strongly influenced by landslide kinematics, Watts et al. (2003a, b) proposed following parameters for slide motion: the characteristic length (s_0), characteristic time (t_0), the terminal velocity (u_t), and the terminal acceleration (a_0) of the slide. The characteristic wavelength in Eq. 2 is given by $\lambda_0 = \frac{u_t}{a_0}\sqrt{gd}$. Here, for each of the 100 scenarios, we calculated these parameters to derive the surface elevations based on the formulas presented by Watts et al. (2005). Equation 2 estimates the initial water surface at the end of the generation phase (t_0) and will be used as an initial condition for the wave propagation toward the coastline. This technique is of paramount importance thanks to its quick and accurate real-time tsunami hazard assessment compared with other two-dimensional depth averaged, or three-dimensional models, which take days of computation to define the initial wave projection at the end of the generation phase (Horrillo et al. 2013; Ma et al. 2013). In Fig. 3, the 3-dimensional waveform for the most voluminous scenario at location 1 is illustrated. This technique has been successfully applied to several landslide/slump tsunami cases in recent years (Watts et al. 2003a, b; Tappin et al. 2008; Abadie et al. 2012).

In the second stage for simulating tsunami propagation, the COMCOT numerical package (Cornell Multi-grid Coupled Tsunami Model) (Liu et al. 1998; Wang and Liu 2006) is employed. It applies the staggered leap-frog finite difference method to solve the nonlinear shallow water equations. The initial tsunami wave at the end of the generation phase is fed as an initial condition to the propagation model and the wave heights are estimated at the coastline and at the two major cities in the region, Chabahar, and Muscat. We exclude run-up calculations in our numerical simulations since it necessitates a high-resolution nearshore topography.

Landslide-generated waves are mostly considered as dispersive and nonlinear as they usually generate shorter wavelength and higher local wave height. Although COMCOT does not take into account the physical frequency dispersion, the leap-frog scheme has an inherent numerical dispersion in it that can artificially compensate with the absence of physical dispersion (Yoon 2002). Because of this, COMCOT is considered as a weakly dispersive model in the literature (Heidarzadeh et al., 2014). Generally, more accurate models that incorporate the frequency dispersion term like fully dispersive Boussinesq model, Navier–Stokes models, or non-hydrostatic type of models are computationally more expensive. On the other hand, the nonlinear shallow water models as a fast alternative have been widely applied by researchers to simulate different landslide-generated tsunamis all around the world, and the results were successfully in agreement with the observed wave heights in the events (Yavari-Ramshe

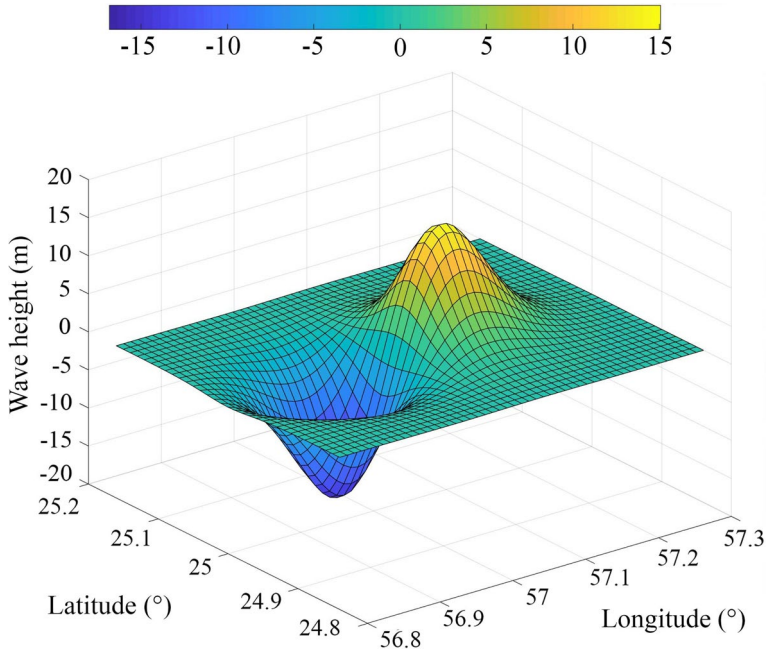

Fig. 3 The 3D waveform of the initial surface water elevation for the worst-case scenario (40 km.^{3}) at location 1

and Ataie-Ashtiani 2016). Additionally, the frequency dispersion is dependent on parameters like depth and distance from the coastline. In turn, the importance of the frequency dispersion depends on the specific cases simulated. For example, Gylfadóttir (2017) showed that frequency dispersion is needed for simulating the tsunami wave radiation pattern for a subaerial landslide tsunami. Glimsdal et al. (2013) suggested a parameter to quantify the importance of dispersion in the propagation of waves originating from the deep ocean for different cases. However, we confine the scope of this research to use nonlinear shallow water model to save computational costs as we simulate 100 scenarios on a large domain.

For bathymetry, we use the 30 Arc-second data set from General Bathymetric Charts of the Oceans (GEBCO)-2014 digital atlas for tsunami modeling, which is provided by the Intergovernmental Oceanographic Commission (IOC) and is computationally suitable for simulating 100 scenarios on the domain (Fig. 1) (Weatherall et al. 2015). This grid was used in both the generation and wave propagation phase toward the shoreline. All the simulations are performed for a total run time of 6 h. In order to make sure that the numerical scheme is stable and converges to the correct solution, we start the simulation with a short time step of 1 s. This helps guarantee the stability of the model under the Courant–Friedrichs–Lewy (CFL) conditions. The CFL is a key parameter for the stability of the numerical schemes while trying to solve partial differential equations (Courant et al. 1928). The stability condition of the model is defined as:

$$\Delta t \leq \frac{\Delta x}{\sqrt{2gh_{max}}} \tag{3}$$

where g is the gravitational acceleration, Δt is the time step, and h_{max} is the maximum water depth in the grid level. COMCOT will automatically adjust the time step to satisfy the CFL condition with the maximum time step fixed at $0.35\Delta x/\sqrt{gh_{max}}$ for the nonlinear shallow water model (Wang and Power, 2011). A Manning's roughness coefficient of 0.013 was used in the simulations and assumed to be constant throughout the bathymetry. This value was successfully used in previous studies to simulate tsunami wave propagation over a sandy bed (Arcement et al. 1989; Huang et al. 2009; Li et al. 2012; Syamsidik et al. 2019).

4 Results and discussion

Figure 4a, b, c, d shows the propagation of worst-case scenarios for Chabahar and Muscat in different time steps, while Fig. 4e,f shows the maximum positive tsunami wave height for the worst-case scenarios for both cities (5.4 m for Chabahar; 6.1 m for Muscat). The worst-case scenarios stem from the largest slump volumes at locations 8 for Chabahar and 19 for Muscat. The associated time series for Chabahar and Muscat during the worst-case scenarios are shown in Fig. 4g,h. It is clear that landslide-generated waves, although large initially, deteriorate quickly and most of their energy is dissipated during the propagation stage. Moreover, the effect of the tsunami source plays a significant role in wave propagation patterns. For landslide-generated tsunamis, the wave heights decay as the as the initial wave begins to propagate from approximately a point source and continues in all directions within the domain (Ruffini et al. 2019). In fact, the decay in wave height is not only because the generated waves are dispersive, but also the wave heights generally decay as waves propagate with semi-circular fronts from the source. This is different from seismically generated tsunamis with longer source types. As expected, the first waves reaching the coast are negative in amplitude (Fig. 4 g,h). This is due to the direction of submarine mass movements since all our scenarios occur toward deeper water. For comparison, the parameters and the simulated wave heights of previous simulated landslide-generated waves and one of our analogous scenarios are summarized in Table 3.

Figure 5 shows the distribution of maximum wave heights at the coast, and Fig. 6 shows the average positive wave height at the computational grid point during the entire tsunami simulation time. Wave heights reach to more than 6 m along the Iranian coast during some scenarios. However, these events seem to be rare since there is a huge gap between the maximum and average result (the average wave height is lower than 1 m across the entire study domain). On the other hand, Oman's coastal regions may experience significant waves during landslide-generated tsunamis, with peak wave height up to 6.5 m, and average wave height up to about 3 m in some places. Thus, Oman's coastal regions may be more vulnerable to landslide-generated waves generated in the western Makran than the coastlines of Iran or Pakistan. This is likely partly due to steep nearshore bathymetry along Oman's coast and the fact that the steep bathymetry is close to Oman's coast. According to Fig. 2, slope angles are more than 20 degrees in some parts, making it critical and hazardous for a huge submarine landslide. Regarding the tsunamis that initiate from a mass movement in the deep ocean, results show that the slump with an approximate volume of 40 km^3 at location 23 (Fig. 2) can generate wave heights of 1.5 m at Oman's coastline. This reveals that submarine landslides in deep water, although less probable, can still generate considerable wave heights if the slump is significantly large and close enough to the coastline.

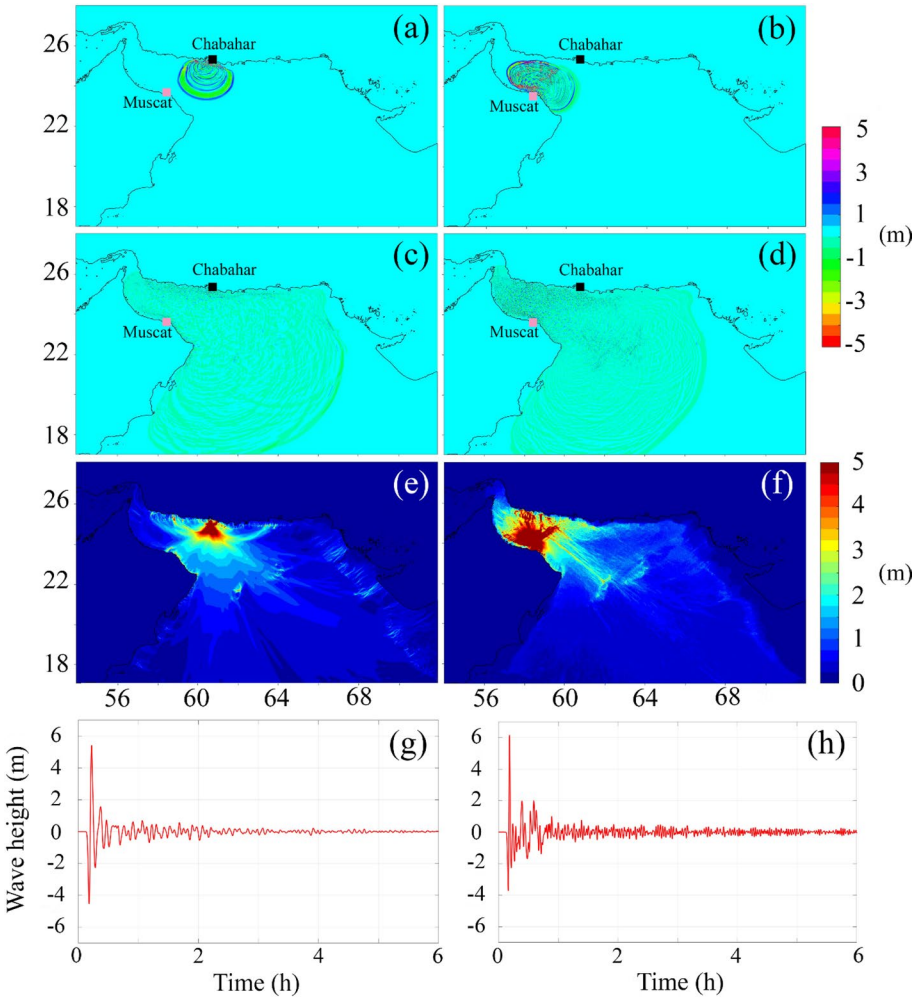

Fig. 4 Snapshots of the simulation of worst-case scenarios for Chabahar, black square **a**,**c** and Muscat, pink square **b**,**d** after 10 min and 45 min, respectively. Figures **e** and **f** show the maximum wave height that every nodes experience during the worst-case scenarios for Chabahar and Muscat. **g** and **h** are the simulated time series in Chabahar and Muscat for 6 h of simulation

Another point to be mentioned is that the average wave amplitude in the far-field regions like the eastern coast of Pakistan and off of Oman is very small. Landslide-generated waves generally do not travel long distances due to their dispersive nature. Besides, for the far-field zone in the southern part of Oman, most of the energetic waves are concentrated in the headland part of Oman and the less energetic waves are propagating toward the far-field in the southern part of Oman. According to the directivity of tsunami propagation, landslide-generated tsunami waves tend to radiate their energy in the mass failure direction (Okal 2003). As the generated waves in western Makran are propagating toward the southern part of Oman, due to the effect of refraction in waves, most of the wave energies are concentrated in the headland, off of Muscat, and the smaller waves propagate toward the southern part of Oman (Fig. 6). In addition, small wave heights in the far-field can be

Table 3 Submarine landslide parameters of previous events

Scenario	Location(°E) (°N)	Length (km)	Width (km)	Thickness (m)	Approximate volume(km^3)	Wave height at chabahar (m)	Wave height at muscat (m)
2013[a]	61.49°E 24.62°N	10–15	10–15	100	Not reported	0.25	0.45
1945[b]	63.0°E 24.8°N	15	15	600	40	2	Not reported
Location17	24.5°E 61.5°N	8	8	800	20	0.3	0.35

[a]According to (Heidarzadeh and Satake 2014)

[b]According to (Heidarzadeh and Satake 2017a)

attributed to the driving force of the tsunami beginning from a small source point in the domain and dispersing as it travels in the direction of the far-field (Ruffini et al. 2019). Because of the mentioned reasons, the effect of landslide-generated waves in the far-field is negligible.

In deterministic tsunami hazard assessment for areas with minimal clues of potential locations for tsunamigenic mass failures, it is important to presume several credible hypothetical scenarios and compare the maximum wave heights and the average wave height as an index for the likelihood of the worst-case scenario. The considerable gap between the maximum and average wave height at some locations, like some parts of the Iranian coastline in our simulations, can be interpreted as landslide-generated waves do not seem to pose a severe hazard to those parts of the domain. In other words, the likelihood of the worst-case scenario and its associated huge wave amplitudes in those areas seems to be low. It is worth noting that assuming unreasonable hypothetical scenarios may sometime lead to an overestimation of tsunami hazard. For example, Nouri et al. (2020) tried to conduct a deterministic assessment of submarine landslide hazards in western Makran by modeling the 1998 Papua New Guinea event as a worst-case scenario. They assumed the seafloor slope gradient as their criteria for locating the hypothetical worst-case scenario and simulated the associated landslide-generated tsunami on the steepest slope in the region. Therefore, the results of their simulation seem to be overestimated as they got the maximum wave amplitude at Muscat to be around 24 m. This huge wave height at the Muscat was due to the fact that their hypothetical landslide location was on the steepest location of the continental shelf and very close to Muscat. However, we already know that such voluminous submarine landslides generally do not occur on such steep slopes as the thick layer of unconsolidated failure-prone sediments does not usually accumulate on slopes steeper than 15° (Masson et al. 2006a). To avoid this kind of overestimate, geological, sedimentological, and geotechnical studies and field work are needed to for finding the potential submarine landslide locations and defining the worst-case scenarios (Shynkarenko et al. 2022). In this article, due to the huge gap between maximum and average wave height, we can conclude that assuming wave heights as huge as 5.5 m can be considered an overestimation for Chabahar.

Figure 7 shows the histogram of wave heights at Chabahar and Muscat. The results of the simulations indicate that 64 percent of trials bring small waves (wave heights lower than 0.5 m) to Chabahar, while 46 percent of trials bring small waves to Muscat. This is

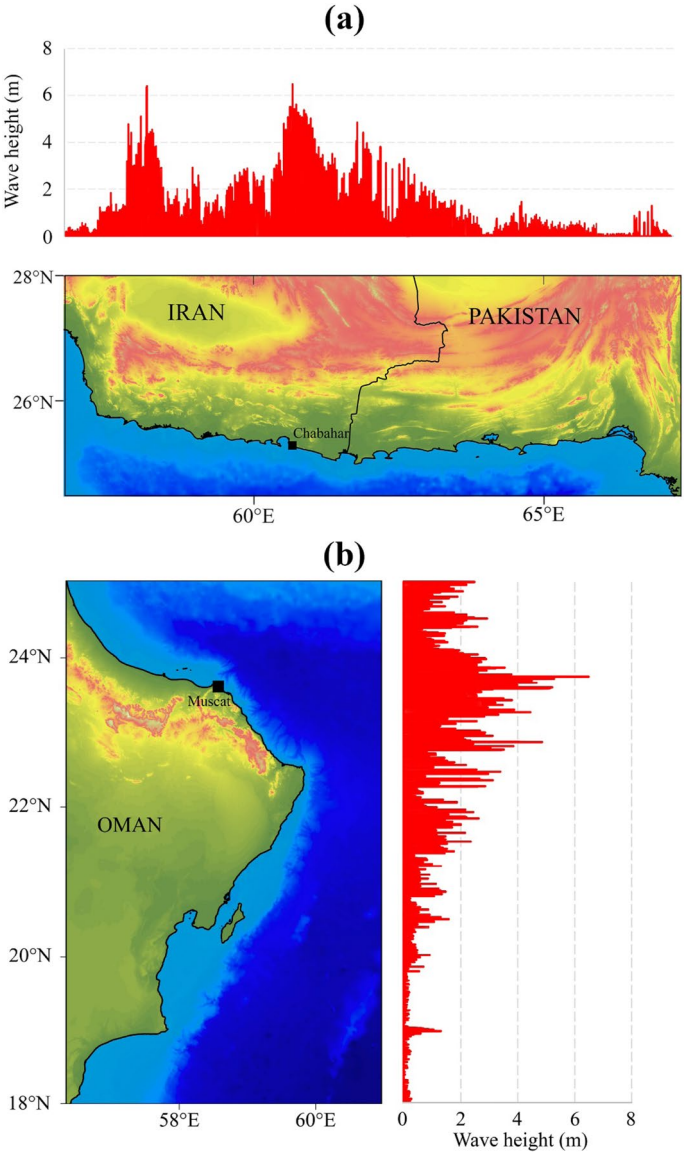

Fig. 5 Distribution of maximum positive wave height along the coastlines of Iran and Pakistan **a**, and Oman **b** due to all scenarios

mainly because of the great distance between the cities' and scenario's source locations, and small slope angles in some locations. On the other hand, two percent and 13 percent of scenarios would create dangerous waves (wave heights larger than 2 m) for Chabahar and Muscat, respectively. Only if the submarine landslide is huge (greater than 40 km^3) and close enough to the city can it produce devastating effects in the coastal cities. By taking into account all the scenarios, the average wave height at Chabahar and Muscat are 0.5 m, and 1.7 m, respectively. Although Chabahar can experience dangerous waves

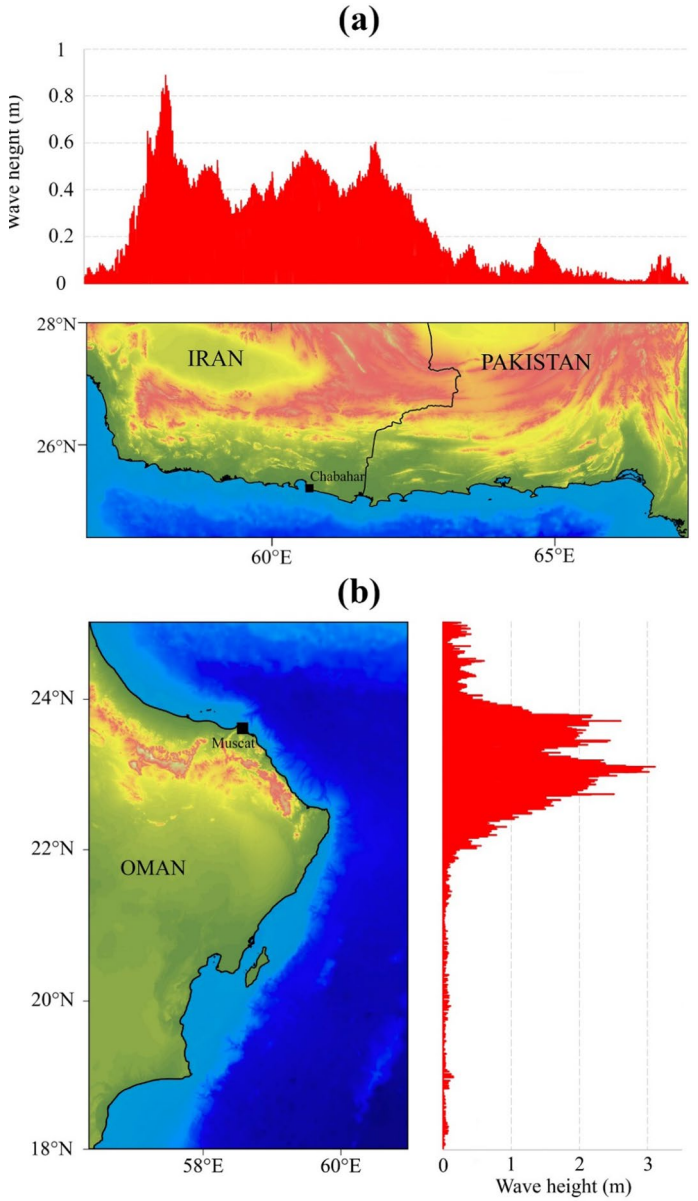

Fig. 6 Distribution of average wave height along the coastlines of Iran, Pakistan **a**, and Oman **b** due to all scenarios

during a few scenarios, the difference between the maximum and average illuminates that most of the scenarios do not pose any serious hazard in that part of the domain. On the other hand, the considerable average wave height for Muscat shows that this city is more vulnerable to landslide-generated tsunamis and can experience some huge waves

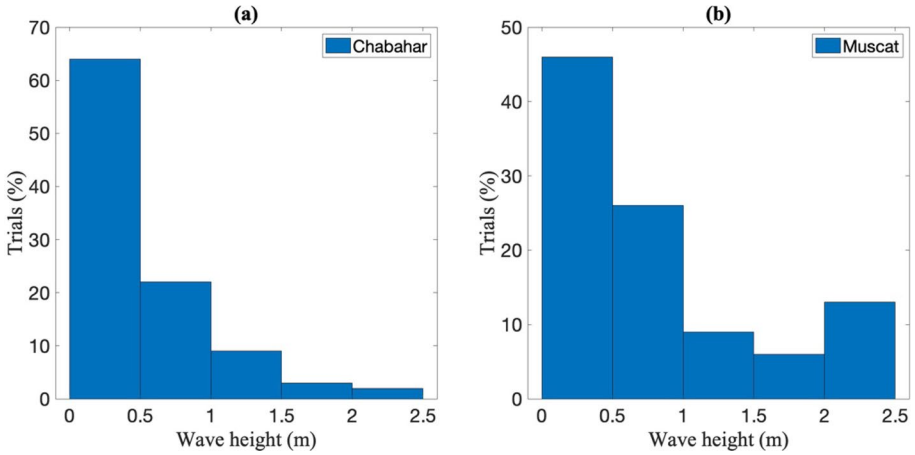

Fig. 7 Histograms of wave heights at Chabahar **a** and Muscat **b** for all scenarios

during several scenarios. This also confirms our previous finding that Muscat seems to be more susceptible to landslide-generated tsunamis.

5 Conclusion

We investigated the effects of submarine landslide-generated waves on coastlines in western Makran. To avoid unrealistic worst-case scenarios and hazard assessment by assuming a single worst-case scenario, we simulated different scenarios with landslide volumes varying from 10 to 40 km^3 in 25 different locations. The results of our simulations reveal that although most of the scenarios do not create waves larger than 0.5 m, both Chabahar, Iran and Muscat, Oman experience severe waves during some scenarios and that Oman's coastline is more vulnerable to landslide-generated waves. As all the simulated scenarios in this paper were hypothetical, we concluded that Iran's coastline seems to be less vulnerable to huge landslide-generated tsunami waves because of the large gap between the maximum and average wave height in all scenarios. For a better understanding of the level of hazard related to submarine landslides for future tsunami hazard mitigation programs, more geological, geotechnical, and sedimentological studies are required in western Makran. In recent years, the main focus of tsunami research centers has been earthquake-generated tsunamis in the region. This study reveals that the effect of submarine landslide-generated waves is not negligible and should be taken into account in future tsunami hazard assessment studies in the region. Moreover, if any of the tsunamigenic earthquakes are accompanied by a landslide in the region, it would escalate the situation and would possibly lead to run-ups that are greater than what would be expected for earthquake-generated tsunamis. A probabilistic approach for determining hazard assessments for submarine landslide tsunamis or a new machine-learning approach can shed more light on the hazard of landslide-generated waves in the region. Additionally, having the ability to more accurately locate previous landslides using geological and bathometric data and simulate them using more accurate models for the generation and propagation phase can provide insight into potential consequences of tsunamis and can inform risk management decisions.

Acknowledgements The authors would like to thank the developers of COMCOT program (Wang, 2009). Some of the figures were created using the Generic Mapping Tools (Wessel et al., 2019) and Mirone (Luis, 2007). This manuscript was greatly benefited from very detailed and constructive comments from Dave Tappin and two anonymous reviewers. AR's work was supported by the Université Savoie Mont Blanc through the internal AAP Recherche (2021) NAMI project. The first author would like to express his gratitude to Doctor Chris Lashley and Emily Chapman for their valuable feedback, which greatly contributed to improving this manuscript.

Funding This study is supported by Natural Sciences and Engineering Research Council (NSERC) DG 2020-04207.

Declarations

Conflict of interest The authors have no conflicts of interests to declare that are relevant to the content of this article.

References

Abadie SM, Harris JC, Grilli ST, Fabre R (2012) Numerical modeling of tsunami waves generated by the flank collapse of the Cumbre Vieja Volcano (La Palma, Canary Islands): Tsunami source and near field effects. J Geophys Res: Oceans 117(5):1–26. https://doi.org/10.1029/2011JC007646

Arcement GJ, Schneider VR (1989) Guide for selecting Manning's roughness coefficients for natural channels and flood plains. In Water Supply Paper. https://doi.org/10.3133/wsp2339

Bourget J, Zaragosi S, Ellouz-Zimmermann S, Ducassou E, Prins MA, Garlan T, Lanfumey V, Schneider JL, Rouillard P, Giraudeau J (2010) Highstand vs lowstand turbidite system growth in the Makran active margin: imprints of high-frequency external controls on sediment delivery mechanisms to deep water systems. Marine Geol 274(1–4):187–208. https://doi.org/10.1016/j.margeo.2010.04.005

Brune S, Babeyko AY, Gaedicke C, Ladage S (2010) Hazard assessment of underwater landslide-generated tsunamis: a case study in the Padang region. Indonesia Nat Hazards 53(2):205–218. https://doi.org/10.1007/s11069-009-9424-x

Byrnet D, Syigs A, Davis D (1992) Great thrust earthquakes and aseismic slip along the plate boundary of the Makran subductionzone. J Geophys Res 97:449–478

Courant R, Friedrichs K, Lewy H (1928) Über die partiellen Differenzengleichungen der mathematischen Physik. Math Ann 100(1):32–74. https://doi.org/10.1007/BF01448839

Ellouz-Zimmermann N, Lallemant SJ, Castilla R, Mouchot N, Leturmy P, Battani A, Buret C, Cherel L, Desaubliaux G, Deville E, Ferrand J, Lügcke A, Mahieux G, Mascle G, Mühr P, Pierson-Wickmann A-C, Robion P, Schmitz J, Danish M, Tabreez A (2007) Offshore Frontal Part of the Makran Accretionary Prism: The Chamak Survey (Pakistan). In: Lacombe O, Roure F, Lavé J, Vergés J (eds) Thrust Belts and Foreland Basins. Springer, Berlin Heidelberg, pp 351–366

Fauzi A, Mizutani N (2020) Machine learning algorithms for real-time tsunami inundation forecasting: a case study in Nankai Region. Pure Appl Geophys 177(3):1437–1450. https://doi.org/10.1007/s00024-019-02364-4

Frohling E, Szeliga W (2016) GPS constraints on interplate locking within the Makran subduction zone. Geophys J Int 205(1):67–76. https://doi.org/10.1093/gji/ggw001

Geist EL, Lynett PJ, Chaytor JD (2009) Hydrodynamic modeling of tsunamis from the Currituck landslide. Mar Geol 264(1–2):41–52. https://doi.org/10.1016/j.margeo.2008.09.005

Glimsdal S, Pedersen GK, Harbitz CB, Løvholt F (2013) Dispersion of tsunamis: Does it really matter? Nat Hazard 13:1507–1526. https://doi.org/10.5194/nhess-13-1507-2013

Grando G, Mcclay K (2007) Morphotectonics domains and structural styles in the Makran accretionary prism, offshore Iran. Sed Geol 196:157–179. https://doi.org/10.1016/j.sedgeo.2006.05.030

Grezio A, Babeyko A, Baptista MA, Behrens J, Costa A, Davies G, Geist EL, Glimsdal S, González FI, Griffin J, Harbitz CB, LeVeque RJ, Lorito S, Løvholt F, Omira R, Mueller C, Paris R, Parsons T, Polet J, Thio HK (2017) Probabilistic tsunami hazard analysis: multiple sources and global applications. Rev Geophys 55(4):1158–1198. https://doi.org/10.1002/2017RG000579

Grilli ST, Watts P (2005) Tsunami generation by submarine mass failure I: modeling, experimental validation and sensitivity analyses. J Waterway Port Coastal and Ocean Eng 131(6):283–297. https://doi.org/10.1061/(ASCE)0733-950X(2005)131:6(283)

Grilli ST, Taylor ODS, Baxter CDP, Maretzki S (2009) A probabilistic approach for determining submarine landslide tsunami hazard along the upper east coast of the United States. Mar Geol 264(1–2):74–97. https://doi.org/10.1016/j.margeo.2009.02.010

Grilli ST, O'Reilly C, Harris JC, Bakhsh TT, Tehranirad B, Banihashemi S, Kirby JT, Baxter CDP, Eggeling T, Ma G, Shi F (2015) Modeling of SMF tsunami hazard along the upper US East Coast: detailed impact around Ocean City. MD Natural Hazards 76(2):705–746. https://doi.org/10.1007/s11069-014-1522-8

Gylfadóttir SS, Kim J, Helgason JK, Brynjólfsson S, Höskuldsson Á, Jóhannesson T, Harbitz CB, Løvholt F (2017) The 2014 Lake Askja rockslide-induced tsunami: optimization of numerical tsunami model using observed data. J Geophys Res: Oceans 122(5):4110–4122. https://doi.org/10.1002/2016JC012496

Haider R, Ali S, Hoffmann G, Reicherter K (2023) A multi-proxy approach to assess tsunami hazard with a preliminary risk assessment: A case study of the Makran Coast Pakistan. Marine Geol 459:107032. https://doi.org/10.1016/j.margeo.2023.107032

Harbitz CB, Løvholt F, Bungum H (2014) Submarine landslide tsunamis: How extreme and how likely? Nat Hazards 72(3):1341–1374. https://doi.org/10.1007/s11069-013-0681-3

Heidarzadeh M, Satake K (2014) Possible sources of the tsunami observed in the northwestern Indian ocean following the 2013 September 24 Mw 7.7 Pakistan inland earthquake. Geophys J Int 199(2):752–766. https://doi.org/10.1093/gji/ggu297

Heidarzadeh M, Satake K (2015) New insights into the source of the Makran tsunami of 27 november 1945 from tsunami waveforms and coastal deformation data. Pure Appl Geophys 172(3):621–640. https://doi.org/10.1007/s00024-014-0948-y

Heidarzadeh M, Satake K (2017a) A combined earthquake-landslide source model for the tsunami from the 27 november 1945 Mw 8.1 makran earthquake. Bull Seismol Soc Am 107(2):1033–1040. https://doi.org/10.1785/0120160196

Heidarzadeh M, Satake K (2017b) Possible dual earthquake-landslide source of the 13 November 2016 Kaikoura, New Zealand Tsunami. Pure Appl Geophys 174(10):3737–3749. https://doi.org/10.1007/s00024-017-1637-4

Heidarzadeh M, Krastel, Sebastian;Yalchiner, A. C. (2014) The state-of-the-art numerical tools for modeling landslide tsunamis: a short review. *submarine mass movements and their consequences*. Adv Nat Technol Hazards Res 37:201–212. https://doi.org/10.1007/978-3-319-00972-8

Heidarzadeh M, Pirooz MD, Zaker NH, Yalciner AC, Mokhtari M, Esmaeily A (2008) Historical tsunami in the Makran Subduction Zone off the southern coasts of Iran and Pakistan and results of numerical modeling. Ocean Eng 35(8–9):774–786. https://doi.org/10.1016/j.oceaneng.2008.01.017

Heidarzadeh M, Tappin DR, Ishibe T (2019) Modeling the large runup along a narrow segment of the Kaikoura coast, New Zealand following the November 2016 tsunami from a potential landslide. Ocean Eng 175:113–121. https://doi.org/10.1016/j.oceaneng.2019.02.024

Heidarzadeh M, Gusman AR, Ishibe T, Sabeti R, Šepić J (2022) Estimating the eruption-induced water displacement source of the 15 January 2022 Tonga volcanic tsunami from tsunami spectra and numerical modelling. Ocean Eng 261:112165. https://doi.org/10.1016/j.oceaneng.2022.112165

Higman B, Shugar DH, Stark CP, Ekström G, Koppes MN, Lynett P, Dufresne A, Haeussler PJ, Geertsema M, Gulick S, Mattox A, Venditti JG, Walton MAL, McCall N, Mckittrick E, MacInnes B, Bilderback EL, Tang H, Willis MJ, Loso M (2018) The 2015 landslide and tsunami in Taan Fiord Alaska. Sci Rep 8(1):1–12. https://doi.org/10.1038/s41598-018-30475-w

Hoechner A, Babeyko AY, Zamora N (2016) Probabilistic tsunami hazard assessment for the Makran region with focus on maximum magnitude assumption. Nat Hazard 16(6):1339–1350. https://doi.org/10.5194/nhess-16-1339-2016

Hoffmann G, Al-yahyai S, Naeem G, Kociok M, Grützner C (2014) An Indian Ocean tsunami triggered remotely by an onshore earthquake in Balochistan. Pakistan Geology 42(10):883–886. https://doi.org/10.1130/G35756.1

Horrillo J, Wood A, Kim GB, Parambath A (2013) A simplified 3-D Navier-Stokes numerical model for landslide-tsunami: application to the Gulf of Mexico. J Geophys Res: Oceans 118(12):6934–6950. https://doi.org/10.1002/2012JC008689

Huang Z, Wu T-R, Tan SK, Megawati K, Shaw F, Liu X, Pan T-C (2009) Tsunami hazard from the subduction Megathrust of the South China Sea: part II Hydrodynamic modeling and possible impact on Singapore. J Asian Earth Sci 36(1):93–97. https://doi.org/10.1016/j.jseaes.2008.08.007

Iorio V, Bellotti G, Cecioni C, Grilli ST (2021) A numerical model for the efficient simulation of multiple landslide-induced tsunamis scenarios. Ocean Modell 168:101899. https://doi.org/10.1016/j.ocemod.2021.101899

Kukowski N, Schillhorn T, Huhn K, Von Rad U, Husen S, Flueh ER (2001) Morphotectonics and mechanics of the central Makran accretionary wedge off Pakistan. Mar Geol 173(1–4):1–19. https://doi.org/10.1016/S0025-3227(00)00167-5

Latcharote P, Al-Salem K, Suppasri A, Pokavanich T, Toda S, Jayaramu Y, Al-Enezi A, Al-Ragum A, Imamura F (2018) Tsunami hazard evaluation for Kuwait and Arabian Gulf due to Makran Subduction Zone and Subaerial landslides. Nat Hazards 93(s1):127–152. https://doi.org/10.1007/s11069-017-3097-7

Li L, Qiu Q, Huang Z (2012) Numerical modeling of the morphological change in Lhok Nga, west Banda Aceh, during the 2004 Indian Ocean tsunami: understanding tsunami deposits using a forward modeling method. Nat Hazards 64(2):1549–1574. https://doi.org/10.1007/s11069-012-0325-z

Lindhorst K, Krastel S, Papenberg C, Heidarzadeh M (2014) Modeling submarine landslide-generated waves in lake Ohrid, Macedonia / Albania. Submarine mass movements and their consequences. Adv Nat Technol Hazards Res 37:497–506. https://doi.org/10.1007/978-3-319-00972-8

Liu P L-F, Woo S-B, C. Y.-S. (1998). Computer programs for tsunami propagation and inundation. *Technical Report, School of Civil and Enviromental Engineering, Cornel University*.

Locat J, Lee HJ (2002) Submarine landslides: advances and challenges. Can Geotech J 39(1):193–212. https://doi.org/10.1139/t01-089

Løvholt F, Glimsdal S, Harbitz CB (2020) On the landslide tsunami uncertainty and hazard. Landslides 17(10):2301–2315. https://doi.org/10.1007/s10346-020-01429-z

Luis JF (2007) Mirone: a multi-purpose tool for exploring grid data. Comput Geosci 33(1):31–41. https://doi.org/10.1016/j.cageo.2006.05.005

Ma G, Kirby JT, Shi F (2013) Numerical simulation of tsunami waves generated by deformable submarine landslides. Ocean Modell 69:146–165. https://doi.org/10.1016/j.ocemod.2013.07.001

Masson DG, Harbitz CB, Wynn RB, Pedersen G, Løvholt F (2006a) Submarine landslides : processes triggers and hazard prediction Submarine landslides : processes triggers and hazard prediction. Philos Trans Royal Soc 394:2009–2039. https://doi.org/10.1098/rsta.2006.1810

Masson DG, Harbitz CB, Wynn RB, Pedersen G, Løvholt F (2006b) Submarine landslides: processes, triggers and hazard prediction. Philos Trans Series a, Math, Phys Eng Sci 364(1845):2009–2039. https://doi.org/10.1098/rsta.2006.1810

Mouchot N, Loncke L, Mahieux G, Bourget J, Lallemant S, Ellouz-Zimmermann N, Leturmy P (2010) Recent sedimentary processes along the Makran trench (Makran active margin, off Pakistan). Marine Geol 271(1):17–31. https://doi.org/10.1016/j.margeo.2010.01.006

Mulia IE, Gusman AR, Satake K (2018) Alternative to non-linear model for simulating tsunami inundation in real-time. Geophys J Int 214(3):2002–2013. https://doi.org/10.1093/GJI/GGY238

Mulia IE, Gusman AR, Satake K (2020) Applying a deep learning algorithm to tsunami inundation database of megathrust earthquakes. J Geophys Res: Solid Earth 125(9):e2020JB019690. https://doi.org/10.1029/2020JB019690

Nouri, M., Montazeri Namin, M., & Rashidi, A. (2020). A first-order Landslide Tsunami Hazard Assessment in the Western Makran. *18th Iranian Hydraulic Conference*.

Okal EA (2003) Normal mode energetics for far-field tsunamis generated by dislocations and landslides. Pure Appl Geophys 160(10):2189–2221. https://doi.org/10.1007/s00024-003-2426-9

Okal EA, Fritz HM, Hamzeh MA, Ghasemzadeh J (2015) Field survey of the 1945 Makran and 2004 Indian ocean tsunamis in Baluchistan. Iran Pure and Appl Geophys 172(12):3343–3356. https://doi.org/10.1007/s00024-015-1157-z

Pampell-Manis A, Horrillo J, Shigihara Y, Parambath L (2016) Probabilistic assessment of landslide tsunami hazard for the northern Gulf of Mexico. J Geophys Res: Oceans 121(1):1009–1027. https://doi.org/10.1002/2015JC011261

Pendse CG (1946) The Mekran earthquake of the 28th November 1945. India Meteorol Depart Sci Notes 10(125):141–145

Platt JP, Leggett JK, Young J, Raza H, Alam S (1985) Large-scale sediment underplating in the Makran accretionary prism, southwest Pakistan. Geology 13(7):507–511. https://doi.org/10.1130/0091-7613(1985)13%3c507:LSUITM%3e2.0.CO;2

Pranantyo IR, Heidarzadeh M, Cummins PR (2021) Complex tsunami hazards in eastern Indonesia from seismic and non-seismic sources: deterministic modelling based on historical and modern data. Geosci Lett 8(1):20. https://doi.org/10.1186/s40562-021-00190-y

Rashidi A, Dutykh D, Shomali ZH, Keshavarz Farajkhah N, Nouri M (2020) A review of Tsunami hazards in the Makran subduction zone. Geosciences 10(9):1–31. https://doi.org/10.3390/geosciences10090372

Rastgoftar E, Soltanpour M (2016) Study and numerical modeling of 1945 Makran tsunami due to a probable submarine landslide. Nat Hazards 83(2):929–945. https://doi.org/10.1007/s11069-016-2356-3

Rauter M, Viroulet S, Gylfadóttir SS, Fellin W, Løvholt F (2022) Granular porous landslide tsunami modelling – the 2014 Lake Askja flank collapse. Nat Commun 13(1):678. https://doi.org/10.1038/s41467-022-28296-7

Rodriguez M, Chamot-Rooke N, Hébert H, Fournier M, Huchon P (2013) Owen Ridge deep-water submarine landslides: implications for tsunami hazard along the Oman coast. Nat Hazard 13(2):417–424. https://doi.org/10.5194/nhess-13-417-2013

Ruffini G, Heller V, Briganti R (2019) Numerical modelling of landslide-tsunami propagation in a wide range of idealised water body geometries. Coastal Eng 153:103518. https://doi.org/10.1016/j.coastaleng.2019.103518

Salmanidou DM, Heidarzadeh M, Guillas S (2019) Probabilistic landslide-generated Tsunamis in the Indus Canyon, NW Indian Ocean, using statistical emulation. Pure Appl Geophys 176(7):3099–3114. https://doi.org/10.1007/s00024-019-02187-3

Schwab J, Krastel S, Heidarzadeh M, Brune S (2014) Modeling of Potential Landslide Tsunami Hazards Off Western Thailand (Andaman Sea). In: Krastel S, Behrmann J-H, Völker D, Stipp M, Berndt C, Urgeles R, Chaytor J, Huhn K, Strasser M, Harbitz CB (eds) Submarine Mass Movements and Their Consequences: 6th International Symposium. Springer International Publishing, Cham, pp 517–527

Shynkarenko A, Kremer K, Stegmann S, Bergamo P, Lontsi AM, Roesner A, Hammerschmidt S, Kopf A, Fäh D (2022) Geotechnical characterization and stability analysis of subaqueous slopes in Lake Lucerne (Switzerland). Nat Hazards 113(1):475–505. https://doi.org/10.1007/s11069-022-05310-1

Suppasri A, Latcharote P, Pokavanich T, Al-Salem K, Al-Enezi A, TODA, S., & IMAMURA, F. (2016) Tsunami hazard assessment for the arabian gulf from earthquakes and surface landslides. J Japan Soc Civ Eng Ser B (coastal Engineering) 72(2):1675–1680. https://doi.org/10.2208/kaigan.72.I_1675

Syamsidik T, Suppasri A, Al'Ala, M., Luthfi, M., & Comfort, L. K. (2019) Assessing the tsunami mitigation effectiveness of the planned Banda Aceh Outer Ring Road (BORR), Indonesia. Nat Hazard 19(1):299–312. https://doi.org/10.5194/nhess-19-299-2019

Synolakis CE, Bardet JP, Borrero JC, Davies HL, Okal EA, Silver EA, Sweet S, Tappin DR (2002) The slump origin of the 1998 Papua New Guinea tsunami. Proc Royal Soc a: Math, Phys Eng Sci 458(2020):763–789. https://doi.org/10.1098/rspa.2001.0915

Tan H, Ruffini G, Heller V, Chen S (2018) A numerical landslide-tsunami hazard assessment technique applied on hypothetical scenarios at Es Vedrà, Offshore Ibiza. J Marine Sci Eng 6(4):111. https://doi.org/10.3390/jmse6040111

Tappin DR, Watts P, Grilli ST (2008) The Papua New Guinea tsunami of 17 July 1998: anatomy of a catastrophic event. Nat Hazard 8(2):243–266. https://doi.org/10.5194/nhess-8-243-2008

Tappin DR, Grilli ST, Harris JC, Geller RJ, Masterlark T, Kirby JT, Shi F, Ma G, Thingbaijam KKS, Mai PM (2014) Did a submarine landslide contribute to the 2011 Tohoku tsunami? Marine Geol 357:344–361. https://doi.org/10.1016/j.margeo.2014.09.043

ten Brink US, Geist EL (2021) *On the Use of Statistical Analysis to Understand Submarine Landslide Processes and Assess Their Hazard BT - Understanding and Reducing Landslide Disaster Risk: Volume 1 Sendai Landslide Partnerships and Kyoto Landslide Commitment* (K. In: Mikoš M, Sassa S, Bobrowsky PT, Takara K, Dang K (eds) Sassa. Springer International Publishing, Cham, pp 329–341

Urgeles R, Bahk JJ, Lee SH, Horozal S, Cukur D, Kim SP, Kim GY, Jeong SW, Um IK (2019) Tsunami hazard from submarine landslides: scenario-based assessment in the Ulleung Basin, East Sea (Japan Sea). Geosci J 23(3):439–460. https://doi.org/10.1007/s12303-018-0044-x

Wang X-M (2009) *USER MANUAL FOR COMCOT VERSION 1.7 (FIRST DRAFT)*

Wang X, Liu PL-F (2006) An analysis of 2004 Sumatra earthquake fault plane mechanisms and Indian Ocean tsunami. J Hydraulic Res 44:147–154. https://doi.org/10.1080/00221686.2006.9521671

Wang X, Power WL (2011) *COMCOT : a tsunami generation propagation and run-up model*. GNS Science, GNS Science report

Watts P, Grilli ST, Kirby JT, Fryer GJ, Tappin DR (2003a) Landslide tsunami case studies using a Boussinesq model and a fully nonlinear tsunami generation model. Nat Hazards Earth Syst Sci 3(5):391–402. https://doi.org/10.5194/nhess-3-391-2003

Watts P, Grilli ST, Kirby JT, Fryer GJ, Tappin DR (2003b) *Landslide tsunami case studies using a Boussinesq model and a fully nonlinear tsunami generation model*. 391–402

Watts P, Grilli ST, Tappin DR, Fryer GJ (2005) Tsunami generation by submarine mass failure II: predictive equations and case studies. J Waterway Port Coastal and Ocean Eng 131(6):298–310. https://doi.org/10.1061/(ASCE)0733-950X(2005)131:6(298)

Weatherall P, Marks KM, Jakobsson M, Schmitt T, Tani S, Arndt JE, Rovere M, Chayes D, Ferrini V, Wigley R (2015) A new digital bathymetric model of the world's oceans. Earth and Space Sci 2(8):331–345. https://doi.org/10.1002/2015EA000107

Wessel P, Luis JF, Uieda L, Scharroo R, Wobbe F, Smith WHF, Tian D (2019) The generic mapping tools version 6. Geochem, Geophys, Geosyst 20(11):5556–5564. https://doi.org/10.1029/2019GC008515

Yalciner A, Zaytsev A, Aytore B, Insel I, Heidarzadeh M, Kian R, Imamura F (2014) A Possible submarine landslide and associated tsunami at the Northwest Nile Delta Mediterranean Sea. Oceanography 27(2):68–75. https://doi.org/10.5670/oceanog.2014.41

Yavari-Ramshe S, Ataie-Ashtiani B (2016) Numerical modeling of subaerial and submarine landslide-generated tsunami waves—recent advances and future challenges. Landslides 13(6):1325–1368. https://doi.org/10.1007/s10346-016-0734-2

Yoon SB (2002) Propagation of distant tsunamis over slowly varying topography. J Geophys Res: Oceans. https://doi.org/10.1029/2001JC000791

Zafarani H, Etemadsaeed L, Rahimi M, Kheirdast N, Rashidi A, Ansari A, Mokhtari M, Eskandari-Ghadi M (2023) Probabilistic tsunami hazard analysis for western Makran coasts, south-east Iran. Nat Hazards 115(2):1275–1311. https://doi.org/10.1007/s11069-022-05595-2